1    **Magnetospheric chaos and dynamical complexity response during storm time disturbance**

2    Irewola Aaron Oludehinwa[1], Olasunkanmi Isaac Olusola[1], Olawale Segun Bolaji[1,2], Olumide
3    Olayinka Odeyemi[1], Abdullahi Ndzi Njah[1]

4                               [1]Department of Physics, University of Lagos, Nigeria

5                               [2]Department of Physics, University of Tasmania, Australia

6    **Abstract**

7    In this study, we examine the magnetospheric chaos and dynamical complexity response to the

8    disturbance storm time ($D_{st}$) and solar wind electric field ($VB_s$) during different categories of

9    geomagnetic storm (minor, moderate and major geomagnetic storm). The time series data of the

10   $D_{st}$ and $VB_s$ are analyzed for the period of nine years using nonlinear dynamics tools (Maximal

11   Lyapunov Exponent, MLE, Approximate Entropy, ApEn and Delay Vector Variance, DVV). We

12   found a significant trend between each nonlinear parameter and the categories of geomagnetic

13   storm. The MLE and ApEn values of the $D_{st}$ indicate that chaotic and dynamical complexity

14   responses are high during minor geomagnetic storms, reduce at moderate geomagnetic storms and

15   decline further during major geomagnetic storms. However, the MLE and ApEn values obtained

16   from $VB_s$ indicate that chaotic and dynamical complexity responses are high with no significant

17   difference between the periods that are associated with minor, moderate and major geomagnetic

18   storms. The test for nonlinearity in the $D_{st}$ time series during major geomagnetic storm reveals the

19   strongest nonlinearity features. Based on these findings, the dynamical features obtained in the

20   $VB_s$ as input and $D_{st}$ as output of the magnetospheric system suggest that the magnetospheric

21   dynamics is nonlinear and the solar wind dynamics is consistently stochastic in nature.

22   ***Keywords***: $D_{st}$ signals, Solar wind electric field ($VB_s$) signals, Geomagnetic storm, Chaotic

23   behaviour, Dynamical complexity, Nonlinearity.

## 1.0 Introduction

The response of chaos and dynamical complexity behaviour with respect to magnetospheric dynamics varies (Tsurutani et al., 1990). This is due to changes in the interplanetary electric fields imposed on the magnetopause and those penetrating the inner magnetosphere and sustaining convection thereby initiating geomagnetic storm (Dungey, 1961; Pavlos et al., 1992). A prolonged southward turning of interplanetary magnetic field (IMF, $B_z$), which indicates that solar wind-magnetosphere coupling is in-progress was confirmed on many occasions for which such geomagnetic storm was driven by Corotating Interaction Regions (CIRs), or by the sheath preceding an interplanetary coronal mass ejection (ICME) or by a combination of the sheath and an ICME magnetic cloud (Gonzalez and Tsurutani, 1987; Tsurutani and Gonzalez, 1987; Tsurutani et al., 1988; Cowley, 1995; Tsutomu, 2002; Yurchyshyn et al., 2004; Kozyra et al., 2006; Echer et al., 2008; Meng et al., 2019; Tsurutani et al., 2020). The sporadic magnetic reconnection between the southward component of the Alfven waves and the earth's magnetopause leads to isolated substorms/convection events such as the high intensity long-duration continuous AE activity (HILDCAA) which are shown to last from days to weeks (Akasofu, 1964; Tsurutani et al., 1972; Meng et al., 1973; Tsurutani and Gonzalez, 1987; Hajra et al., 2013; Liou et al., 2013; Mendes et al., 2017; Hajra and Tsurutani, 2018; Tsurutani and Hajra, 2021).  Notably, the introduction of Disturbance Storm Time ($D_{st}$) index (Sugiura, 1964; Sugiura and Kamei, 1991) unveiled the quantitative measure of the total energy of the ring current particles. Therefore, the $D_{st}$ index remains one of the most popular global indicators that can precisely reveal the severity of a geomagnetic storm (Dessler and Parker, 1959).

The $D_{st}$ fluctuations exhibit different signatures for different categories of geomagnetic storm. Ordinarily, one can easily anticipate that fluctuations in a $D_{st}$ signal appear chaotic and complex.

48    These may arise from the changes in the interplanetary electric fields driven by the solar wind-

49    magnetospheric coupling processes. At different categories of geomagnetic storm, fluctuations in

50    the $D_{st}$ signals differ (Oludehinwa et al., 2018). One obvious reason is that as the intensity of the

51    geomagnetic storm increases, the fluctuation behaviour in the $D_{st}$ signal becomes more complex

52    and nonlinear in nature. It has been established that the electrodynamic response of the

53    magnetosphere to solar wind drivers are non-autonomous in nature (Price and Prichard, 1993;

54    Price et al., 1994; Johnson and Wings, 2005).    Therefore, the chaotic analysis of the

55    magnetospheric time series must be related to the concept of input-output dynamical process

56    (Russell et al., 1974; Burton et al.,1975; Gonzalez et al., 1989; Gonzalez et al., 1994).

57    Consequently, it is necessary to examine the chaotic behaviour of the solar wind electric field

58    $(VB_s)$ as input signals and the magnetospheric activity index $(D_{st})$ as output during different

59    categories of geomagnetic storms.

60    Several works have been presented on the chaotic and dynamical complexity behaviour of the

61    magnetospheric dynamics based on autonomous concept, i.e using the time series data of

62    magnetospheric activity alone such as auroral electrojet (AE), Amplitude Lower (AL) and $D_{st}$

63    index (Vassiliadis et al.,1990; Baker and Klimas, 1990; Vassiliadis et al.,1991; Shan et al., 1991;

64    Pavlos et al., 1994; Klimas et al., 1996; Valdivia et al., 2005; Mendes et al., 2017; Consolini,

65    2018). They found evidence of low-dimensional chaos in the magnetospheric dynamics. For

66    instance, the report by Vassiliadis et al. (1991) shows that the computation of Lyapunov exponent

67    for AL index time series gives a positive value of Lyapunov exponent indicating the presence of

68    chaos in the magnetospheric dynamics. Unnikrishnan, (2008) studied the deterministic chaotic

69    behaviour in the magnetospheric dynamics under various physical conditions using AE index time

70    series and found that the seasonal mean value of Lyapunov exponent in winter season during quiet

71 periods $(0.7 \pm 0.11\ min^{-1})$ is higher than that of the stormy periods $(0.36 \pm 0.09\ min^{-1})$.

72 Balasis et al. (2006) examined the magnetospheric dynamics in the $D_{st}$ index time series from

73 pre-magnetic storm to magnetic storm period using fractal dynamics. They found that the transition

74 from anti-persistent to persistent behaviour indicates that the occurrence of an intense geomagnetic

75 storm is imminent. Balasis et al. (2009) further reveal the dynamical complexity behaviour in the

76 magnetospheric dynamics using various entropy measures. They reported a significant decrease in

77 dynamical complexity and an accession of persistency in the $D_{st}$ time series as the magnetic storm

78 approaches. Recently, Oludehinwa et al. (2018) examined the nonlinearity effects in $D_{st}$ signals

79 during minor, moderate and major geomagnetic storm using recurrence plots and recurrence

80 quantification analyses. They found that the dynamics of the $D_{st}$ signal is stochastic during minor

81 geomagnetic storm periods and deterministic as the geomagnetic storm increases.

82 Also, studies describing the solar wind and magnetosphere as a non-autonomous system have been

83 extensively investigated. Price et al. (1994) examine the nonlinear input-output analysis of AL

84 index and different combinations of interplanetary magnetic field (IMF) with solar wind

85 parameters as input functions. They found that only a few of the input combinations show any

86 evidence whatsoever for nonlinear coupling between the input and output for the interval

87 investigated. Pavlos et al. (1999) presented further evidence of magnetospheric chaos. They

88 compared the observational behaviour of the magnetospheric system with the results obtained by

89 analyzing different types of stochastic and deterministic input-output systems and asserted that a

90 low dimensional chaos is evident in magnetospheric dynamics. Devi et al. (2013) studied the

91 magnetospheric dynamics using AL index and the southward component of IMF$(B_z)$. They

92 observed that the magnetosphere and turbulent solar wind have values corresponding to nonlinear

93 dynamical system with chaotic behaviour. The modeling and forecasting approach have been

94 applied to magnetospheric time series using nonlinear models (Valdivia et al., 1996; Vassiliadis et

95 al., 1999; Vassiliadis, 2006; Balikhin et al., 2010). These efforts have improved our understanding

96 that the concept of nonlinear dynamics can reveal some hidden dynamical information in the

97 observational time series. In addition to these nonlinear effects in $D_{st}$ signals, a measure of the

98 exponential divergence and convergence within the trajectories of a phase space known as

99 Maximal Lyapunov Exponent (MLE), which has the potential to depict the chaotic behavior in the

100 $D_{st}$ and $VB_s$ time series during a minor, moderate and major geomagnetic storm have not been

101 investigated. In addition, to the best of our knowledge, computation of Approximate Entropy

102 (ApEn) that depicts the dynamical complexity behaviour during different categories of

103 geomagnetic storm has not been reported in the literature. The test for nonlinearity through delay

104 vector variance (DVV) analysis that reveals the nonlinearity features in $D_{st}$ and $VB_s$ time series

105 during minor, moderate and major geomagnetic storms is not well known. It is worth to note that

106 understanding the dynamical characteristics in the $D_{st}$ and $VB_s$ signals at different categories of

107 geomagnetic storms will provide useful diagnostic information to different conditions of space

108 weather phenomenon. Consequently, this study attempts to carry out comprehensive numerical

109 analyses to unfold the chaotic and dynamical complexity behaviour in the $D_{st}$ and $VB_s$ signals

110 during minor, moderate and major geomagnetic storm. In section 2, our methods of data

111 acquisition are described. Also, the nonlinear analysis that we employed in this investigation are

112 detailed. In section 3, we unveiled our results and engage the discussion of results in section 4.

113 **2.0 Description of the Data and Nonlinear Dynamics**

114 The $D_{st}$ index is derived by measurements from ground-based magnetic stations at low-latitudes

115 observatories around the world and depicts mainly the variation of the ring current, as well as the

116 Chapman-Ferraro Magnetopause currents, and tail currents to a lesser extent (Sugiura, 1964;

117    Feldstein et al., 2005; Feldstein et al., 2006; Love and Gannon, 2009). Due to its global nature, $D_{st}$

118    time series provides a measure of how intense a geomagnetic storm was (Dessel and Parker, 1959).

119    In this study, we considered $D_{st}$ data for the period of nine years from January to December

120    between 2008 and 2016 which were downloaded from the World Data Centre for Geomagnetism,

121    Kyoto, Japan (http://wdc.kugi-kyoto-u.ac.jp/Dstae/index.html). We use the classification of

122    geomagnetic storms as proposed by Gonzalez et al. (1994) such that $D_{st}$ index value in the ranges

123    $0 \leq Dst \leq -50nT,\ -50nT \leq Dst \leq -100nT,\ -100nT \leq Dst \leq -250nT$ are classified as

124    minor, moderate and major geomagnetic storms respectively and each time series is being

125    classified based on its minimum $D_{st}$ value. The solar wind electric field ($VB_s$) data are archived

126    from the National Aeronautics and Space Administration, Space Physics Facility

127    (http://omniweb.gsfc.nasa.gov). The sampling time of $D_{st}$ and $VB_s$ time series data was 1-hour.  It

128    is well known that the dynamics of the solar wind contribute to the driving of the magnetosphere

129    (Burton et al. 1975). Furthermore, we took the solar wind electric field ($VB_s$) as the input signal

130    (Price and Prichard, 1993; Price et al., 1994). The $VB_s$ was categorized according to the periods

131    of minor, moderate and major geomagnetic storm. Then, the $D_{st}$ and $VB_s$ time series were

132    subjected to a variety of nonlinear analytical tools explained as follow:

133    **2.1 Phase Space Reconstruction and Observational time series**

134    An observational time series can be defined as a sequence of scalar measurements of some

135    quantity, which is a function of the current state of the system taken at multiples of a fixed sampling

136    time. In nonlinear dynamics, the first step in analyzing an observational time series data is to

137    reconstruct an appropriate state space of the system. Takens (1981) and Mane (1981) stated that

138    one time series or a few simultaneous time series are converted to a sequence of vectors. This

139   reconstructed phase space has all the dynamical characteristic of the real phase space provided the

140   time delay and embedding dimension are properly specified.

141
$$X(t) = [x(t), x(t + \tau), x(t + 2\tau), \dots, x(t + (m - 1)\tau]^T \qquad (1)$$

142   Where $X(t)$ is the reconstructed phase space, $x(t)$ is the original time series data, $\tau$ is the time

143   delay and $m$ is the embedding dimension. An appropriate choice of $\tau$ and $m$ are needed for the

144   reconstruction of phase space which is determined by average mutual information and false nearest

145   neighbor, respectively.

146   **2.2 Average Mutual Information (AMI)**

147   The method of Average Mutual Information (AMI) is one of the nonlinear techniques used to

148   determine the optimal time delay ($\tau$) required for phase space reconstruction in observational time

149   series. The time delay mutual information was proposed by Fraser and Swinney, (1986) instead of

150   an autocorrelation function. This method takes into account nonlinear correlations within the time

151   series data. It measures how much information can be predicted about one time series point, given

152   full information about the other. For instance, the mutual information between $x_i$ and $x_{(i+\tau)}$

153   quantifies the information in state $x_{(i+\tau)}$ under the assumption that information at the state $x_i$ is

154   known. The AMI for a time series, $x(t_i)$, $i = 1,2, \dots, N$ is calculated as:

155
$$I(T) = \sum_{x(t_i),\ x(t_i+T)} P(x(t_i), x(t_i + T)) \times \log_2 \left[ \frac{P(x(t_i), x(t_i+T))}{P(x(t_i))\, P(x(t_i+T))} \right] \qquad (2)$$

156   where $x(t_i)$ is the $i$th element of the time series, $T = k\Delta t$ $(k = 1,2, \dots, k_{max})$, $P(x(t_i))$ is the

157   probability density at $x(t_i)$, $P(x(t_i), x(t_i + T))$ is the joint probability density at the pair

158   $x(t_i), x(t_i + T)$. The time delay ($\tau$) of the first minimum of AMI is chosen as optimal time delay

159   (Fraser and Swinney, 1986). Therefore, the AMI was applied to the $D_{st}$ and $VB_s$ time series and

160    the plot of AMI versus time delay is shown in Figure (3). We notice that the AMI showed the first

161    local minimum at roughly $\tau = 15hr$. Furthermore, the values of $\tau$ near this value of ~15hr

162    maintain constancy for both $VB_s$ and $D_{st}$. In the analysis $\tau = 15hr$ was used as the optimal time

163    delay for the computation of maximal Lyapunov exponent.

**2.3 False Nearest Neighbor (FNN)**

164

165    In determining the optimal choice of embedding dimension$(m)$, the false nearest neighbor method

166    was used in the study. The method was suggested by Kennel et al. (1992). The concept is based

167    on how the number of neighbors of a point along a signal trajectory changes with increasing

168    embedding dimension. With increasing embedding dimension, the false neighbor will no longer

169    be neighbors, therefore by examining how the number of neighbors changes as a function of

170    dimension, an appropriate embedding dimension can be determined. For instance, suppose we

171    have a one-dimensional time series. We can construct a time series $y(t)$ of $D$-dimensional points

172    from the original one-dimensional time series $x(t)$ as follows:

173
$$y(t) = (x(t), x(t + \tau), \dots, x(t + (D - 1)\tau)) \qquad (3)$$

174    where $\tau$ and $D$ are time delay and embedding dimension. Using the formular from Kennel et al.

175    (1992); Wallot and Monster, (2018), if we have a $D$-dimensional phase space and denote the $rth$

176    nearest neighbor of a coordinate vector $y(t)$ by $y^{(r)}(t)$, then the square of the Euclidean distance

177    between $y(t)$ and the $rth$ nearest neighbor is:

178
$$R_D^2(t, r) = \sum_{k=0}^{D-1} \left[x(t + k\tau) - x^{(r)}(t + k\tau)\right]^2 \qquad (4)$$

179    Now applying the logic outlined above, we can go from a $D$-dimensional phase space to $(D + 1)$

180    dimensional phase space by time-delay embedding, adding a new coordinate to $y(t)$, and ask what

181    is the squared distance between $y(t)$ and the same $rth$ nearest neighbor:

182    $$R_{D+1}^2(t, r) = R_D^2(t, r) + \left[x(t + D\tau) - x^{(r)}(t + D\tau)\right]^2 \qquad (5)$$

183    As explained above, if the one-dimensional time series is already properly embedded in $D$

184    dimensions, then the distance $R$ between $y(t)$ and the $rth$ nearest neighbor should not change

185    appreciably by some distance criterion $R_{tol}(i.e\ R < R_{tol})$. Moreover, the distance of the nearest

186    neighbor when embedded into the next higher dimension relative to the size of the attractor should

187    be less than some criterion $A_{tol}(i.e\ R_{D+1} < A_{tol})$. Doing this for the nearest neighbor of each

188    coordinate will result on many false nearest neighbors when embedding is insufficient or in few

189    (or no) false neighbors when embedding is sufficient. In the analysis, the FNN was applied to the

190    $D_{st}$ and $VB_s$ time series to detect the optimal value of embedding dimension$(m)$. Figure (4) shows

191    a sample plot of the percentage of false nearest neighbor against embedding dimension in one of

192    the months under investigation (other months show similar results, thus for brevity we depict only

193    one of the results). We notice that the false nearest neighbor attains its minimum value at $m \geq 5$

194    indicating that embedding dimension $(m)$ from $m \geq 5$ are optimal values. Therefore, $m = 5$ was

195    used for the computation of maximal Lyapunov exponent.

196    **2.4 Maximal Lyapunov Exponent (MLE)**

197    The Maximal Lyapunov Exponent (MLE) is one of the most popular nonlinear dynamics tool used

198    for detecting chaotic behaviour in a time series data. It describes how small changes in the state of

199    a system grow at an exponential rate and eventually dominate the behaviour. An important

200    indication of chaotic behavior of a dissipative deterministic system is the existence of a positive

201 Lyapunov Exponent. A positive MLE signifies divergence of trajectories in one direction or

202 expansion of an initial volume in this direction. On the other hand, a negative MLE exponent

203 implies convergence of trajectories or contraction of volume along another direction. The

204 algorithm proposed by Wolf et al. (1985) for estimating MLE is employed to compute the chaotic

205 behavior of the $D_{st}$ and $VB_s$ time series at minor, moderate and major geomagnetic storm. Other

206 methods of determining MLE includes Rosenstein's method, Kantz's method and so on. In this

207 study, the MLE at minor, moderate and major geomagnetic storms periods was computed with

208 $m = 5$ and $\tau = 15hr$ as shown in figures (5 & 6-bar plots) for $D_{st}$ and $VB_s$. The calculation of

209 MLE is explained as follows: given a sequence of vector $x(t)$, an $m$-dimensional phase space is

210 formed from the observational time series through embedding theorem as

211
$$\{x(t), x(t + \tau), \dots, x(t + (m - 1)\tau)\} \tag{6}$$

212 where $m$ and $\tau$ are as defined earlier, after reconstructing the observational time series, the

213 algorithm locates the nearest neighbor (in Euclidean sense) to the initial point $\{x(t_0), \dots, x(t_0 +$

214 $(m - 1)\tau\}$ and denote the distance between these two points $L(t_0)$. At a later point $t_1$, the initial

215 length will have evolved to length $L'(t_1)$. Then the MLE is calculated as:

216
$$\lambda = \frac{1}{t_M - t_0} \sum_{k=1}^{M} \log_2 \frac{L'(t_k)}{L(t_{k-1})} \tag{7}$$

217 M is the total number of replacement steps. We look for a new data point that satisfies two criteria

218 reasonably well: its separation, $L(t_1)$, from the evolved fiducial point is small. If an adequate

219 replacement point cannot be found, we retain the points that were being used. This procedure is

220 repeated until the fiducial trajectory has traversed the entire data.

221

222  **2.5 Approximate Entropy (ApEn)**

223  Approximate Entropy (ApEn) is one of the nonlinear dynamics tools that measure the dynamical

224  complexity in observational time series. The concept was proposed by Pincus, (1991) which

225  provides a generalized measure of regularity, such that it accounts for the logarithm likehood in

226  the observational time series. For instance, a dataset of length, $N$, that repeat itself for $m$ points

227  within a boundary will again repeat itself for $m + 1$ points. Because of its computational

228  advantage, ApEn has been widely used in many areas of disciplines to study dynamical complexity

229  (Pincus and Kalman (2004); Pincus and Goldberger (1994); McKinley et al. (2011); Kannathan et

230  al. (2005); Balasis et al. (2009); Shujuan and Weidong, (2010); Moore and Marchant (2017)). The

231  ApEn is computed using the formula below:

232  $$ApEn(m, r, N) = \frac{1}{N-m+1} \sum_{i=1}^{N-m+1} \log C_i^m(r) - \frac{1}{N-m} \sum_{i=1}^{N-m} \log C_i^m(r) \qquad (8)$$

233  where $C_i^m(r) = \frac{1}{N-m+1} \sum_{j=1}^{N-m+1} \Theta(r - \|x_i - x_j\|)$ is the correlation integral, $m$ is the embedding

234  dimension and $r$ is the tolerance. To compute the ApEn for the $D_{st}$ and $VB_s$ time series classified

235  as minor, moderate and major geomagnetic storm from 2008 to 2016, we choose $(m = 3, \tau =$

236  $1hr)$. We refer the works of Pincus, (1991); Kannathal et al. (2005); and Balasis et al. (2009) to

237  interested readers where all the computational steps regarding ApEn were explained in details.

238  Figures (5 & 6) depict the stem plot of ApEn for $D_{st}$ and $(VB_s)$ from 2008 to 2016.

239  **2.6 Delay Vector Variance (DVV) analysis**

240  The Delay Vector Variance (DVV) is a unified approach in analyzing and testing for nonlinearity

241  in a time series (Gautama et al., 2004; Mandic et al., 2007). The basic idea of the DVV is that, if

242  two delay vectors of a predictable signal are close to each other in terms of the Euclidean distance,

243 they should have similar target. For instance, when a time delay ($\tau$) is embedded into a time series

244 $x(k)$, $k = 1,2, ..., N$, then a reconstructed phase space vector is formed which represents a set of

245 delay vectors (DVs) of a given dimension.

$$X(k) = [X_{k-m\tau}, ..., X_{k-\tau}]^T \tag{9}$$

246

247 Reconstructing the phase space, a set ($\lambda_k$) is generated by grouping those DVs that are with a

248 certain Euclidean distance to DVs $(X(k))$. For a given embedding dimension ($m$), a measure of

249 unpredictability $\sigma *^2$ is computed over all pairwise Euclidean distance between delay vector as

$$d(i,j) = \|x(i) - x(j)\| \quad (i \neq j) \tag{10}$$

250

251 Then, sets $\lambda_k(r_d)$ are generated as the sets which consist of all delay vectors that lie closer to $x(k)$

252 than a certain distance $r_d$.

$$\lambda_k(r_d) = \{x(i)\|x(k) - x(i)\| \leq r_d\} \tag{11}$$

253

254 For every set $\lambda_k(r_d)$, the variance of the corresponding target $\sigma *^2 (r_d)$ is

$$\sigma *^2 (r_d) = \frac{\frac{1}{N}\sum_{k=1}^{N} \sigma_k^2(r_d)}{\sigma_k} \tag{12}$$

255

256 where $\sigma *^2 (r_d)$ is target variance against the standardized distance indicating that Euclidean

257 distance will be varied in a manner standardized with respect to the distribution of pairwise

258 distance between DVs. Iterative Amplitude Adjusted Fourier Transform (IAAFT) method is used

259 to generate the surrogate time series (Kugiumtzis, 1999). If the surrogate time series yields DV

260 plots similar to the original time series and the scattered plot coincides with the bisector line, then

261 the original time series can be regarded as linear (Theiler et al., 1992; Gautama et al., 2004; Imitaz,

262 2010; Jaksic et al., 2016). On the other hand, if the surrogate time series yields DV plot that is not

263     similar to that of the original time series, then the deviation from the bisector lines indicates

264     nonlinearity. The deviation from the bisector lines grows as a result of the degree of nonlinearity

265     in the observational time series.

266
$$t^{DVV} = \sqrt{\langle(\sigma^{*2}(r_d) - \frac{\Sigma_{i=1}^{N}\sigma_{s,i}^{*2}}{N_s})\rangle} \tag{13}$$

267     where $\sigma_{s,i}^{*2}(r_d)$ is the target variance at the span $r_d$ for the $i^{th}$ surrogate. To carry out the test for

268     nonlinearity in the $D_{st}$ signals, $m = 3$ and $n_d = 3$, the number of reference DVs=200, and number

269     of surrogate, $N_s = 25$ was used in all the analysis. Then we examined the nonlinearity response at

270     minor, moderate and major geomagnetic storm.

**3.0 Results**

In this study, $D_{st}$ and $VB_s$ time series from January to December were analyzed for the period of nine years (2008 to 2016) to examine the chaotic and dynamical complexity response in the magnetospheric dynamics during minor, moderate and major geomagnetic storms. Figures (1) & (2), display the samples of fluctuation signatures of $D_{st}$ and $VB_s$ signals classified as (a): minor, (b): moderate and (c): major geomagnetic storms. The plot of Average Mutual information against time delay ($\tau$) shown in Figure (3) depicts that the first local minimum of the AMI function was found to be roughly at $\tau = 15$hr. Furthermore, we notice that the values of $\tau$ near this value of (~15hr) maintain constancy for both $VB_s$ and $D_{st}$. Also, in Figure (4), we display the plot of the percentage of false nearest neighbor against embedding dimension ($m$). It is obvious that a decrease in false nearest neighbor when increasing the embedding dimension drop steeply to zero at the optimal dimension($m = 5$), thereafter the false neighbors stabilizes at that $m = 5$ for $VB_s$ and $D_{st}$. Therefore, $m = 5$ and $\tau = 15$hr was used for the computation of MLE at different categories of geomagnetic storm, while $m = 3$ and $\tau = 1$hr are applied for the computation of ApEn values.

The results of MLE (bar plot) and ApEn (stem plot) for $D_{st}$ at minor, moderate and major geomagnetic storms are shown in Figure 5. During minor geomagnetic storms, we notice that the value of MLE ranges between 0.07 and 0.14 for most of the months classified as minor geomagnetic storm. Similarly, the ApEn (stem plot) ranges between 0.59 and 0.83. It is obvious that strong chaotic behaviour with high dynamical complexity are associated with minor geomagnetic storms. During moderate geomagnetic storms, (see b part of Figure 5), we observe a reduction in MLE values $(0.04 - 0.07)$ compared to minor geomagnetic storm periods. Within the observed values of MLE during moderate geomagnetic storms, we found a slight rise of MLE

294    in the following months (Mar 2008), (Apr 2011), (Jan 2012, Feb 2012, Apr 2012), (Jul 2015, Aug

295    2015, Sept 2015, Oct 2015, Nov 2015) and (Nov 2016). Also, the ApEn revealed a reduction in

296    values between 0.44 and 0.57 during moderate geomagnetic storms. The lowest values of ApEn

297    were noticed in the following months: May 2010, Mar 2011, and Jan 2016. During major

298    geomagnetic storms as shown in Figure 5, the minimum and maximum value of MLE is

299    respectively 0.03 and 0.04 implying a very strong reduction of chaotic behaviour compared with

300    minor and moderate geomagnetic storms. The lowest values of MLE were found in the months of

301    Jul 2012, Jun 2013 and Mar 2015. Interestingly, further reduction in ApEn value $(0.29 - 0.40)$

302    was as well noticed during this period. Thus, during major geomagnetic storms, chaotic behaviour

303    and dynamical complexity subside significantly.

304    We display in Figure 6, the results of MLE and ApEn computation for the $VB_s$ which has been

305    categorized according to the periods of minor, moderate and major geomagnetic storms. The

306    values of MLE (bar plot) were between 0.06 and 0.20 for $VB_s$. The result obtained indicate strong

307    chaotic behaviour with no significant difference in chaoticity during minor, moderate and major

308    geomagnetic storm. Similarly, the results obtained from computation of ApEn (stem plot) for $VB_s$

309    depict a minimum value of 0.60 and peak value of 0.87 as shown in Figure 6. The ApEn values of

310    $VB_s$ indicates high dynamical complexity response with no significant difference during the

311    periods of the three categories of geomagnetic storm investigated.

312    The test for nonlinearity in the $D_{st}$ signals during minor, moderate and major geomagnetic storms

313    was analyzed through the DVV analysis. Shown in Figure 9 is the DVV plot and DVV scatter plot

314    during minor geomagnetic storm for January 2009 and January 2014. We found that the DVV

315    plots during minor geomagnetic storms reveals a slight separation between the original and

316    surrogate data. Also, the DVV scatter plots shows a slight deviation from the bisector line between

317 the original and surrogate data which implies nonlinearity. Also, during moderate geomagnetic

318 storms, we notice that the DVV plot depicts a wide separation between the original and the

319 surrogate data. Also, a large deviation from the bisector line between the original and the surrogate

320 data was also noticed in the DVV scatter plot as shown in Figure (8) thus indicating nonlinearity.

321 In Figure (9), we display samples of DVV plot and DVV scatter plot during major geomagnetic

322 storm for Oct 2011 and Dec 2015. The original and the surrogate data showed a very large

323 separation in the DVV plot during major geomagnetic storm. While the DVV scatter plot depict

324 the greatest deviation from the bisector line between the original and the surrogate data which is

325 also an indication of nonlinearity. The DVV analysis of the $VB_s$ time series during minor, moderate

326 and major geomagnetic storms shown in Figures (10-12) revealed a separation between the original

327 and surrogate data with no significant difference between the periods of minor, moderate and major

328 geomagnetic storm.

329 **4.0 Discussion of Results**

330 **4.1 The chaotic and dynamical complexity response in $D_{st}$ at minor, moderate and major**

331 **geomagnetic storms**

332 Our result shows that the values of MLE for $D_{st}$ during minor geomagnetic storm are higher,

333 indicating significant chaotic response during minor geomagnetic stormy periods (bar plot, Figure

334 5). This increase in chaotic behaviour for $D_{st}$ signals during minor geomagnetic storms may be as

335 a result of asymmetry features in the longitudinal distribution of solar source region for the

336 Corotating Interaction Regions (CIR) signatures responsible for the development of geomagnetic

337 storms (Turner et al. 2006; Kozyra et al. 2006). CIR generated magnetic storms are generally

338 weaker than ICME/MC generated storms (Gonzalez et al., 1994; Tsurutani et al., 1995; Feldstein

339 et al., 2006; Richardson and Cane, 2011). Therefore, we suspect that the increase in chaotic

340 behaviour during minor geomagnetic storms is strongly associated with the asymmetry features in

341 the longitudinal distribution of solar source region for the Corotating Interaction Regions (CIR)

342 signatures. For most of these periods of moderate geomagnetic storms, the values of MLE

343 decreases compared to minor geomagnetic storms. This revealed that as geomagnetic stormy

344 events build up, the level of unpredictability and sensitive dependence on initial condition (chaos)

345 begin to decrease (Lorentz, 1963; Stogaz, 1994). The chaotic behaviour during major geomagnetic

346 storms decreases significantly compared with moderate geomagnetic storms. The reduction in

347 chaotic response during moderate and its further declines at major geomagnetic storms may be

348 attributed to the disturbance in the interplanetary medium driven by sheath preceding an

349 interplanetary coronal mass ejection (ICME) or combination of the sheath and an ICME magnetic

350 cloud (Echer et al., 2008; Tsurutani et al., 2003; Meng et al., 2019).  Notably, the dynamics of the

351 solar wind-magnetospheric interaction are dissipative chaotic in nature (Pavlos, 2012); and, the

352 electrodynamics of the magnetosphere due to the flux of interplanetary electric fields had a

353 significant impact on the state of the chaotic signatures. For instance, the observation of strong

354 chaotic behaviour during minor geomagnetic storms suggests that the dynamics was characterized

355 by a weak magnetospheric disturbance. While the reduction in chaotic behaviour at moderate and

356 major geomagnetic storm period reveals the dynamical features with regards to when a strong

357 magnetospheric disturbance begins to emerge. Therefore, our observation of chaotic signatures at

358 different categories of geomagnetic storm has potential capacity to give useful diagnostic

359 information about monitoring space weather events. It is important to note that the features of $D_{st}$

360 chaotic behaviour at different categories of geomagnetic storm has not been reported in the

361 literature. For example, previous study of Balasis et al. (2009, 2011) investigate dynamical

362 complexity behaviour using different entropy measures and revealed the existence of low

363   dynamical complexity in the magnetospheric dynamics and attributed it to ongoing large

364   magnetospheric disturbance (major geomagnetic storm). The work of Balasis et al. (2009, 2011)

365   where certain dynamical characteristic evolved in the $D_{st}$ signal was revealed was limited to one

366   year data (2001). It is worthy to note that the year 2001, according to sunspot variations is a period

367   of high solar activity during solar cycle 23. It is characterized by numerous and strong solar

368   eruptions that were followed by significant magnetic storm activities. This confirms that on most

369   of the days in year 2001, the geomagnetic activity is strongly associated with major geomagnetic

370   storms. The confirmation of low dynamical complexity response in the $D_{st}$ signal during major

371   geomagnetic storms agree with our current study. However, the idea of comparing the dynamical

372   complexity behaviour at different categories of geomagnetic storms and reveal its chaotic features

373   was not reported. This is the major reason why our present investigation is crucial to the

374   understanding of the level of chaos and dynamical complexity involved during different categories

375   of geomagnetic storms. As an extension to the single-year investigation done by Balasis et al.

376   (2009, 2011) during a major geomagnetic storm, we further investigated nine years data of $D_{st}$

377   that covered minor, moderate and major geomagnetic storms (see Figure 5, stem plots) and

378   unveiled their dynamical complexity behaviour. During major geomagnetic stormy periods, we

379   found that the ApEn values decrease significantly, indicating reduction in the dynamical

380   complexity behaviour. This is in agreement with the low dynamical complexity reported by Balasis

381   et al. (2009, 2011) during a major geomagnetic period. Finally, based on the method of DVV

382   analysis, we found that test of nonlinearity in the $D_{st}$ time series during major geomagnetic storms

383   reveals the strongest nonlinearity features.

384

385

**4.2 The chaotic and dynamical complexity behaviour in the $VB_s$ as input signals.**

The results of the MLE values for $VB_s$ revealed a strong chaotic behaviour during the three categories of geomagnetic storms. Comparing these MLE values during minor to those observed during moderate and major geomagnetic storms, the result obtained did not indicate any significant difference in chaoticity (bar plots, Figure 6). Also, the ApEn values of $VB_s$ during the periods associated with minor, moderate and major geomagnetic storms revealed high dynamical complexity behaviour with no significant difference between the three categories of geomagnetic storms investigated. These observation of high chaotic and dynamical complexity behaviour in the dynamics of $VB_s$ may be due to interplanetary discontinuities caused by the abrupt changes in the interplanetary magnetic field direction and plasma parameters (Tsurutani et al., 2010). Also, the indication of high chaotic and dynamical complexity behaviour in $VB_s$ signifies that the solar wind electric field is stochastic in nature. The DVV analysis for $VB_s$ revealed nonlinearity features with no significant difference between the minor, moderate and major geomagnetic storms. It is worth mentioning that the dynamical complexity behaviour for $VB_s$ is different from what was observed for $D_{st}$ time series data. For instance, our results for $D_{st}$ times series revealed that the chaotic and dynamical complexity behaviour of the magnetospheric dynamics are high during minor geomagnetic storms, reduce at moderate geomagnetic storms and further decline during major geomagnetic storms. While the $VB_s$ signal revealed a high chaotic and dynamical complexity behaviour at all the categories of geomagnetic storm period. Therefore, these dynamical features obtained in the $VB_s$ as input signal and the $D_{st}$ as the output in describing the magnetosphere as a non-autonomous system further support the finding of Donner et al. (2019) that found increased or not changed in dynamical complexity behaviour for $VB_s$ and low dynamical complexity

408    behaviour during storm using recurrence method. Thus, suggesting that the magnetospheric

409    dynamics is nonlinear and the solar wind dynamics is consistently stochastic in nature.

410    **5.0 Conclusions**

411    This work has examined the magnetospheric chaos and dynamical complexity behaviour in the

412    disturbance storm time ($D_{st}$) and solar wind electric field ($VB_s$) as input during different categories

413    of geomagnetic storms. The chaotic and dynamical complexity behaviour at minor, moderate and

414    major geomagnetic storms for solar wind electric field ($VB_s$) as input and $D_{st}$ as output of the

415    magnetospheric system were analyzed for the period of 9 years using nonlinear dynamics tools.

416    Our analysis has shown a noticeable trend of these nonlinear parameters (MLE and ApEn) and the

417    categories of geomagnetic storm (minor, moderate and major). The MLE and ApEn values of the

418    $D_{st}$ have indicated that the chaotic and dynamical complexity behaviour are high during minor

419    geomagnetic storms, low during moderate geomagnetic storms and further reduced during major

420    geomagnetic storms. The values of MLE and ApEn obtained from $VB_s$ indicate that chaotic and

421    dynamical complexity are high with no significant difference during the periods of minor,

422    moderate and major geomagnetic storms. Finally, the test for nonlinearity in the $D_{st}$ time series

423    during major geomagnetic storms reveals the strongest nonlinearity features. Based on these

424    findings, the dynamical features obtained in the $VB_s$ as input and $D_{st}$ as output of the

425    magnetospheric system suggest that the magnetospheric dynamics is nonlinear and the solar wind

426    dynamics is consistently stochastic in nature.

427

428

429

**7.0 Acknowledgement**

The authors would like to acknowledge the World Data Centre for Geomagnetism, Kyoto, and the

National Aeronautics and Space Administration, Space Physics Facility (NASA) for making the

Dst data and solar wind plasma data available for research purpose. Also, the efforts of anonymous

reviewers in ensuring that the quality of the work is enhanced are highly appreciated.

**Declaration of Interest statement**

The authors declare that there is no conflicts of interest.

**References**

Akasofu, S.I., (1964), The development of the auroral substorm. Planet. Space Sci., 12, 273-282, doi:10.1016/0032-0633(64)90151-5.

Baker, D.N., Klimas, A.J., (1990). The evolution of weak to strong geomagnetic activity: An interpretation in terms of deterministic chaos. J. GeoPhys. Res. Letts. Vol. 17, No. 1, PP. 41-44.

Balasis, G., Daglis, I.A., Anastasiadia, A., Eftaxias, K., (2011). Detection of dynamical complexity changes in Dst time series using entropy concepts and rescaled range analysis. W.Liu, M. Fujimoto (eds.), The Dynamics Magnetosphere, IAGA Special Sopron Book Series 3, doi: 10.1007/978-94-007-0501-2_12, Springer Science+Business Media B.V. 2011.

Balasis, G., I.A. Daglis, C. Papadimitriou, M. Kalimeri, A. Anastasiadis, K. Eftaxias (2009). Investigating dynamical complexity in the magnetosphere using various entropy measures, J.Geophys.Res., 114, A0006, doi: 10.1029/2008JA 014035.

450  Balasis, G., I.A. Daglis, P. Kapiris, M.Mandea, D. Vassilliadis, K. Eftaxias (2006). From pre-storm

451  activity to magnetic storms: a transition described in terms of fractal dynamics, Ann.Geophys.,

452  24, 3557-3567, www.ann-geophys.net/24/3557/2006.

453  Balikhin, M.A., Boynton, R.J., Billings, S.A., Gedalin, M., Ganushkina, N., Coca, D., (2010). Data

454  based quest for solar wind-magnetosphere coupling function, Geophys.Res.Lett, 37, L24107,

455  doi: 10.1029/2010GL045733.

456  Burton, R.K., McPherron, R.L., Russell, C.T., (1975). An empirical relationship between

457  interplanetary conditions and Dst. Journal of Geophysical Research, Vol.80, No.31.

458  Consolini, G., (2018), Emergence of dynamical complexity in the Earth's magnetosphere, Machine

459  learning techniques for space weather, PP. 177-202, doi: 10.1016/B978-0-12-811788-0.00007-

460  X

461  Cowley, S.W.H., (1995). The earth's magnetosphere: A brief beginner's guide, EOS

462  Trans.Am.GeoPhys.Union, 76, 525.

463  Dessler, A.J., Parker, E.N., (1959). Hydromagnetic theory of magnetic storm. J. GeoPhys. Res, 64,

464  PP 2239-2259.

465  Devi, S.P., Singh, S.B., Sharma, A.S., (2013). Deterministic dynamics of the magnetosphere:

466  results of the 0-1 test. Nonlin. Processes Geophys., 20, 11-18, 2013, www.nonlin-processes-

467  geophys.net/20/11/2013, doi: 10. 5194/npg-20-11-2013.

468  Donner, R.V., Balasis, G., Stolbova,V., Georgiou, M., Weiderman, M., Kurths, J. (2019).

469  Recurrence-based quantification of dynamical complexity in the earth's magnetosphere at

470    geospace storm time scales. Journal of Geophysical Research: Space Physics, 124, 90-108,

471    doi: 10.1029/2018JA025318.

472  Dungey, J.W., (1961). Interplanetary magnetic field and auroral zones. Phys.Rev.Lett., 6, 47, doi:

473    10.1103/PhysRevLett.6.47

474  Echer, E., Gonzalez, D., Alves, M.V., (2006). On the geomagnetic effects of solar wind

475    interplanetary magnetic structures. Space Weather, Vol.4, S06001,

476    doi:10.1029/2005SW000200.

477  Echer, E., Gonzalez, W.D., Tsurutani, B.T., Gonzalez, A. L. C., (2008), Interplanetary conditions

478    causing intense geomagnetic storms ($D_{st} \leq -100nT$) during solar cycle 23 (1996–2006), J.

479    Geophys. Res., 113, A05221, doi:10.1029/2007JA012744.

480  Feldstein, Y.I., Levitin, A.E., Kozyra, J.U., Tsurutani, B.T., Prigancova, L., Alperovich, L.,

481    Gonzalez, W.D., Mall, U., Alexeev, I.I., Gromava, L.I., Dremukhina, L.A., (2005). Self-

482    consistent modelling of the large-scale distortions in the geomagnetic field during the 24-27

483    September 1998 major geomagnetic storm. JGR, 110, A11214, doi: 10.1029/2004JA010584.

484  Feldstein, Y.I., Popov, V.A., Cumnock, J.A., Prigancova, A., Blomberg, L.G., Kozyra, J.U.,

485    Tsurutani, B.T., Gromova, L.I., Levitin, A.E., (2006). Auroral electrojets and boundaries of

486    plasma domains in the magnetosphere during magnetically disturbed intervals. Ann. Geophys.,

487    24, 2243-2276, www.ann-geophys.net/24/2243/2006/

488  Fraser, A.M., (1986). Using mutual information to estimate metric entropy, dimension and

489    entropies in chaotic system, Springer-Verlag, 1986, PP: 82-91.

490  Fraser, A.M., Swinney, H.L., (1986). Independent coordinates for strange attractors from mutual

491      information, Phys.Rev.A 33, 1134-1140.

492  Gautama, T., Mandic, D.P., Hulle, M.M.V., (2004). The delay vector variance method for detecting

493      determinism and nonlinearity in time series. Physica D, 190, 167-176, doi:

494      10.1016/j.physd.2003.11.001.

495  Gonzalez, W.D., Joselyn, J.A., Kamide, Y., Kroehl, H.W., Rostoker, G., Tsurutani, B.T.,

496      Vasyliunas, V.M., (1994). What is a geomagnetic storm?  J. Geophys. Res.: Space Physics,

497      Vol. 99, issue A4, pg. 5771-5792, doi: 10.1029/93JA02867.

498  Gonzalez, W.D., Tsurutani, B.T., (1987). Criteria of interplanetary parameters causing intense

499      magnetic     storm     $(Dst < -100nT)$.      Planetary      and      Space      Science,

500      https://ntrs.nasa.gov/search.jsp?R=198800068.

501  Gonzalez, W.D., Tsurutani, B.T., Gonalez, A.L.C., Smith, E.J., Tang, F., Akasofu, S.I., (1989).

502      JGR, 94, A7, 8835-8851, doi: 10.1029/JA094iA07p08835.

503  Hajra, R., Echer, E., Tsurutani, B.T., Gonazalez, W.D., (2013). Solar cycle dependence of High-

504      intensity Long-duration Continuous AE activity (HILDCAA) events, relativistic electron

505      predictors? (2013), JGR, Space Physics, 118, 5626-5638, doi: 10.1002/jgra.50530.

506   Hajra, R., Tsurutani, B.T., (2018), Interplanetary shocks inducing magnetospheric supersubstorms

507      (SML<-2500nT): unusual auroral morphologies and energy flow. The AstroPhysical Journal,

508      858:123(6pp), doi:10.3847/1538-4357/aabaed.

509   Horne, R.H., Glauert, S.A., Meredith, N.P., Boscher, D., Maget, V., Heynderickx, D., and Pitcford,

510       D. (2013). Space weather impacts on satellites and forecasting the Earths electron radiation

511       belts with SPACECAST.  Space weather, **11,** 169 - 186

512   Imtiaz, A., (2010). Detection of nonlinearity and stochastic nature in time series by delay vector

513       variance method, International journal of Engineering & Technology, Vol. 10, No. 02.

514   Jaksic, V., Mandic, D.P., Ryan, K., Basu, B., Pakrashi V., (2016). A Comprehensive Study of the

515       Delay Vector Variance Method for Quantification of Nonlinearity in dynamical Systems.

516       *R.Soc.OpenSci.*, 2016: 3:150493, http://dx.doi.org/10.1098/rsos.150493.

517   Johnson, J.R., Wing, S., (2005), A solar cycle dependence of nonlinearity in magnetospheric

518       activity. J. Geophys. Res., 110, A04211, doi: 10.1029/2004JA010638.

519   Kannathal, N., M.L. Choo, U. R. Acharya, P. K. Sadasivan (2005). Entropies for detecting of

520       epilepsy in EEG, Computer Methods and Programs in Biomedicine (2005) 80, 187-194,

521       www.intl.elsevierhealth.com/journals/cmpb.

522   Kennel, M.B., R. Brown, H.D.I. Abarbanel (1992). Determining embedding dimension for phase-

523       space reconstruction using a geometrical construction, PHYSICAL REVIEW A, Volume 45,

524       Number 6.

525   Klimas, A.J., Vassilliasdis, D., Baker. D.N., Roberts, D.A., (1996). The organized nonlinear

526       dynamics of the magnetosphere. J. GeoPhys. Res. Vol.101, No. A6, PP 13089-13113.

527   Kozyra, J.U., Crowley, G., Emery, B.A., Fang, X., Maris, G., Mlynczak, M.G., Niciejewski, R.J.,

528       Palo, S.E., Paxton, L.J., Randall, C.E., Rong, P.P., Russell, J.M., Skinner, W., Solomon, S.C.,

529       Talaat, E.R., Wu, Q., Yee, J.H., (2006), Response of the Upper/Middle Atmosphere to Coronal

530    Holes and Powerful High-Speed Solar Wind Streams in 2003, Geophysical Monograph Series
531    167, 10.1029/167GM24.

532    Kugiumtzis, D., (1999). Test your surrogate before you test your nonlinearity, Phys. Rev. E, 60,
533    2808-2816.

534    Liou, K., Newell, P.T., Zhang, Y.-L., Paxton, L.J., (2013), Statistical comparison of isolated and
535    non-isolated auroral substorms. J. Geophys. Res. Space Physics, 118, 2466-2477, doi:
536    10.1002/jgra.50218.

537    Lorenz, E.N., (1963). Determining nonperiodic flow. J. Atmos.Sci.,20,130.

538    Love, J.J., Gannon, J.L. (2009). Revised Dst and the epicycles of magnetic disturbance: 1958-2007.
539    Ann.GeoPhys., 27, 3101-3131.

540    Mandic, D.P., Chen, M., Gautama, T., Van Hull, M.M., Constantinides, A., (2007). On the
541    Characterization of the Deterministic/Stochastic and Linear/Nonlinear Nature of Time Series.
542    *Proc.R.Soc*, 2008: A464, 1141-1160, doi: 10.1098/rspa. 2007.0154.

543    Mane, R., (1981). On the dimension of the compact invariant sets of certain nonlinear maps, D.Rand
544    and L.S.Young, eds, 1981.

545    Mckinley, R.A., Mclntire, L.K., Schmidt, R., Repperger, D.W., Caldwell, J.A., (2011). Evaluation
546    of Eye Metrics as a Detector of Fatigue. Human factor, 53 (4): 403-414, doi:
547    10.1177/0018720811411297.

548    Mendes, O., Domingues, M.O., Echer, E., Hajra, R., Menconi, V. E., (2017). Characterization of
549    high-intensity, long-duration continuous auroral activity (HILDCAA) events using recurrence

550    quantification analysis. Nonlin. Processes Geophys., 24, 407-417, doi: 10.5194/npg-24-407-

551    2017.

552 Mendes, O., Dominques, M.O., Echer, E., Hajra, R., Menconi, V.E., (2017), Characterization of

553    high-intnesity, long-duration continuous auroral activitiy (HILDCAA) events using

554    recurrence quantification analysis. Nonlin. Processes Geophys.,24,407-417, doi:10.5194/npg-

555    24-407-2017.

556 Meng, C. I., Tsurutani, B., Kawasaki, K., Akasofu, S. I., (1973), Cross-correlation analysis of the

557    AE index and the interplanetary magnetic field Bz component. Journal of Geophysical

558    Research, Vol. 78., No 4., doi: 10.1029/JA078i004p00617.

559 Meng, X., Tsurutani, B. T., Mannucci, A. J. (2019). The solar and interplanetary causes of

560    superstorms (minimum Dst $\leq -250$ nT) during the space age. Journal of Geophysical Research:

561    Space Physics, 124, 3926–3948. https://doi.org/10.1029/2018JA026425.

562 Millan, H., Gharbarian-Alavijeh, B., Garcia-Fornaris, I., (2010). Nonlinear dynamics of mean daily

563    temperature and dewpoint time series at Babolsar, Iran, 1961-2005. Elsevier, Atmospheric

564    Research 98 (2010) 89-101, doi: 10.1016/j.atmosres.2010.06.001.

565 Moore, C., Marchant, T., (2017). The approximate entropy concept extended to three dimensions

566    for calibrated, single parameter structural complexity interrogation of volumetric images.

567    Physics in Medicine & Biology, 62(15).

568 Oludehinwa, I.A., Olusola, O.I., Bolaji, O.S., Odeyemi, O.O., (2018). Investigation of nonlinearity

569    effect during storm time disturbance, Adv. Space. Res, 62 (2018) 440-456, doi:

570    10.1016/j.asr.2018.04.032.

571    Omkar, P.T., Verma, P.L., (2013). Solar features and solar wind plasma parameters with

572        geomagnetic storms during the period of 2002-2006. Indian Journal of Applied Research,

573        Vol.3, Issue.5, ISSN-2249-555X.

574    Pavlos, G.P., (1994). The magnetospheric chaos: a new point of view of the magnetospheric

575        dynamics. Historical evolution of magnetospheric chaos hypothesis the past two decades.

576        Conference Proceeding of the 2nd Panhellenic Symposium held in Democritus University of

577        Thrace, Greece, 26-29, April, edited 1994.

578    Pavlos, G.P., (2012). Magnetospheric dynamics and Chaos theory

579    Pavlos, G.P., Athanasiu, M.A., Diamantidis, D., Rigas, A.G., Sarri, E.T., (1999). Comments and

580        new results about the magnetospheric chaos hypothesis. Nonlinear Processes in Geophysics

581        (1999) 6: 99-127.

582    Pavlos, G.P., Rigas, A.G., Dialetis, D., Sarris, E.T., Karakatsanis, L.P., Tsonis, A.A., (1992).

583        Evidence of chaotic dynamics in the outer solar plasma and the earth magnetosphere. Chaotic

584        dynamics: Theory and Practice, Edited by T. Bountis, Plenum Press, New York, Page. 327-

585        339, doi:10.1007/978-1-4615-3464-8_30.

586    Pincus, S.M., (1991). Approximate entropy as a measure of system complexity, Proc.Natl.Acad.Sci.

587        USA, Vol.88, PP. 2297-2301.

588    Pincus, S.M., Goldberger, A.L., (1994). Physiological time series analysis: what does regularity

589        quantify, The American Journal of Physiology, 266 (4): 1643-1656.

590    Pincus, S.M., Kalman, E.K., (2004). Irregularity, volatility, risk, and financial market time series, Proceedings of the National Academy of Sciences, 101 (38): 13709-13714, doi: 10.1073/pnas.0405168101.

593    Price, C.P., Prichard, D., Bischoff, J.E., (1994). Nonlinear input/output analysis of the auroral electrojet index. Journal of Geophysical Research, Vol.99, No: A7, PP: 227-238.

595    Price,C.P., Prichard, D., (1993). The Non-linear response of the magnetosphere: 30 October, 1978. Geophysical Research Letters, Vol.20.

597    Richardson, I.G., Cane, H.V., (2011), Geoeffectiveness ($D_{st}$ $and$ $K_p$) of interplanetary coronal mass ejections during 1995-2009 and implication for storm forecasting, Space Weather, 9, S07005, doi:10.1029/2011SW000670.

600    Russell, C.T., (2001). Solar wind and Interplanetary Magnetic Field: A Tutorial. Space Weather, Geophysical Monograph 125, Page: 73-89.

602    Russell, C.T., McPherron, R.L., Burton, R.K. (1974). On the cause of geomagnetic storms, J.GeoPhys.Res., 79, 1105-1109.

604    Shujuan G., Weidong, Z., (2010). Nonlinear feature comparison of EEG using correlation dimension and approximate entropy, 3rd international conference on biomedical engineering and informatics.

607    Strogatz, S.H., (1994), Nonlinear dynamics and chaos with Application to physics, Biology, chemistry and Engineering, New York, John Wiley & Sons.

609    Sugiura, M. (1964). Hourly Values of equatorial Dst for the IGY, Ann.Int. GeoPhys. Year, 35, 9-45.

611    Takens, F., (1981). Detecting Strange Attractors in Turbulence in Dynamical Systems, D.*Rand &*

612        *L.Young Eds*, 1981: 898, 366-381.

613    Theiler, J., Eubank, S., Longtin, A., Galdrikian, B., Farmer, J.D., (1992), Testing for nonlinearity

614        in time series: The method of surrogate data, Physica D, 58, 77.

615    Tsurutani, B. T., Meng, C. I., (1972), Interplanetary magnetic field variations and substorm activity.

616        Journal of Geophysical Research, Vol. 77., No 16., doi: 10.1029/JA077i016p029.

617    Tsurutani, B.T., Gonazalez, W.D., (1987), The cause of High-intensity Long duration Continuous

618        AE activity (HILDCAAs): Interplanetary Alfven trains. Planet. Space Sci., 35, 4, 405-412, doi:

619        10.1016/0032-0633(87)90097-3.

620    Tsurutani, B.T., Gonzalez, A.L.C., Tang, F., Arballo, J.K., Okada, M., (1995), Interplanetary origin

621        of geomagnetic activity in the declining phase of the solar cycle. JGR, 100, A11, 717-733,

622        95JA01476.

623    Tsurutani, B.T., Gonzalez, W. D., Tang, F., Akasofu, S.I., Smith, E.J., (1988), Origin of

624        Interplanetary Southward Magnetic Fields Responsible for Major Magnetic Storms Near Solar

625        Maximum (1978-1979), Journal of Geophysical Research, Vol. 93, No. A8, Pages 8519-8531,

626        Paper number 7A9404, 0148-0227/88/007 A-9404$05.00.

627    Tsurutani, B.T., Gonzalez, W.D., Lakhina, G.S. Alex, S., (2003). The extreme magnetic storm of

628        1-2 September 1859, J. Geophys. Res. 108(A7), doi: 10.1029/2002JA009504.

629    Tsurutani, B.T., Hajra, R., (2021). The interplanetary and magnetospheric causes of

630        geomagnetically induced currents (GICs) >10A in the Mantsala finland Pipeline: 1999

631        through 2019. J. Space Weather Space Clim, 11, 23, doi: 10.1051/swsc/2021001.

632    Tsurutani, B.T., Lakhina, G.S., Hajra, R., (2020), The physics of space weather/solar-terrestrial

633       physics (STP): what we know now and what the current and future challenges are, Nonlin.

634       Processes Geophys., 27, 75–119, doi:10.5194/npg-27-75-2020.

635    Tsurutani, B.T., Lakhina, G.S., Verkhoglyadova, O.P., Gonzalez, W.D., Echer, E., Guarnieri, F.L.,

636       (2010). A review of interplanertary discontinuities and their geomagnetic effects. Journal of

637       Atmospheric and Solar-Terrestrial Physics, doi: 10.1016/j.jastp.2010.04.001.

638    Tsurutani, B.T., Sugiura, M., Iyemori, T., Goldstein, B.E., Gonazalez, W.D., Akasofu, S.I., Smith,

639       E.J., (1990). The nonlinear response of AE to the IMF Bs driver: A spectral break at 5 hours.

640       Geophysical Research Letters, Vol.17, No.3., Pages: 279-283.

641    Tsutomu, N., (2002). Geomagnetic storms. Journal of communications Research Laboratory, Vol.

642       49, No.3.

643    Turner, N.E., Mitchell, E.J., Knipp, D.J., Emery, B.A., (2006), Energetics of magnetic storms

644       driven by corotating interaction regions: a study of geoeffectiveness, Geophysical Monograph

645       Series 167, 10.1029/167GM11.

646    Unikrishnan, K., (2008). Comparison of chaotic aspect of magnetosphere under various physical

647       conditions using AE index time series. Ann. Geophys., 26, 941-953, www.ann-

648       geophys.net/26/941/2008.

649    Unikrishnan, K., Ravindran, S., (2010). A study on chaotic behaviour of equatorial/low latitude

650       ionosphere over indian sub-continent, using GPS-TEC time series, J. Atmos. Sol. Ter. Phys.,

651       72, 1080-1089.

652   Valdivia, J.A., Rogan, J., Munoz, V., Gomberoff, L., Klimas, A., Vassilliasdis, D., Uritsky, V.,

653        Sharma, S., Toledo, B., Wastaviono, L. (2005). The magnetosphere as a complex system. Adv.

654        Space. Res, 35, 961-971.

655   Valdivia, J.A., Sharma, A.S., Papadopoulos, K., (1996). Prediction of magnetic storms by nonlinear

656        models. Geophysical Research Letters, 23(21), 2899-2902, doi: 10.1029/96GL02828.

657   Vassiliadis, D., (2006). Systems theory for geospace plasma dynamics, Rev.Geophys., 44, RG2002,

658        doi: 10.1029/2004RG000161.

659   Vassiliadis, D., Klimas, A.J., Valdivia, J.A., Baker, D.N., (1999). The geomagnetic response as a

660        function of storm phase and amplitude and solar wind electric field. Journal of Geophysical

661        Research, 104(A11), 24957-24976, doi: 10.1029/1999JA900185.

662   Vassilliadis, D., Sharma, A.S., Papadopoulos, K., (1991). Lyapunov exponent of magnetospheric

663        activity from AL time series. J. GeoPhys. Letts, Vol. 18, No.8, PP. 1643-1646.

664   Vassilliadis, D.V., Sharma, A.S., Eastman, T.E., Papadopoulou, K., (1990). Low-dimensional

665        chaos in magnetospheric activity from AE time series. J. GeoPhys.Res.Lett, 17, 1841-1844.

666   Wallot, S., Monster, D., (2018). Calculation of Average Mutual Information (AMI) and False

667        Nearest Neigbhours (FNN) for the estimation of embedding parameters of multidimensional

668        time series in MATLAB. Front. Physchol. 9:1679, doi: 10.3389/fpsyg.2018.01679.

669   Watari, S., (2017). Geomagnetic storms of cycle 24 and their solar sources, Earth, Planets and

670        Space, PP: 69:70, doi: 10.1186/s40623-017-0653-z.

671   Wolf, A., Swift, J. B., Swinney, H. L., and Vastano, J. A. (1985). Determining Lyapunov exponents

672        from a time series, *Physica D*, *16*, 285–317, doi:10.1016/0167-2789(85)90011-9.

673    Zhang, J., Dere, K.P., Howard, R.A., Bothmer, V., (2002), Identification of solar sources of major

674        geomagnetic storms between 1996 and 2000. Astrophysical Journal, 582:520-53.

675
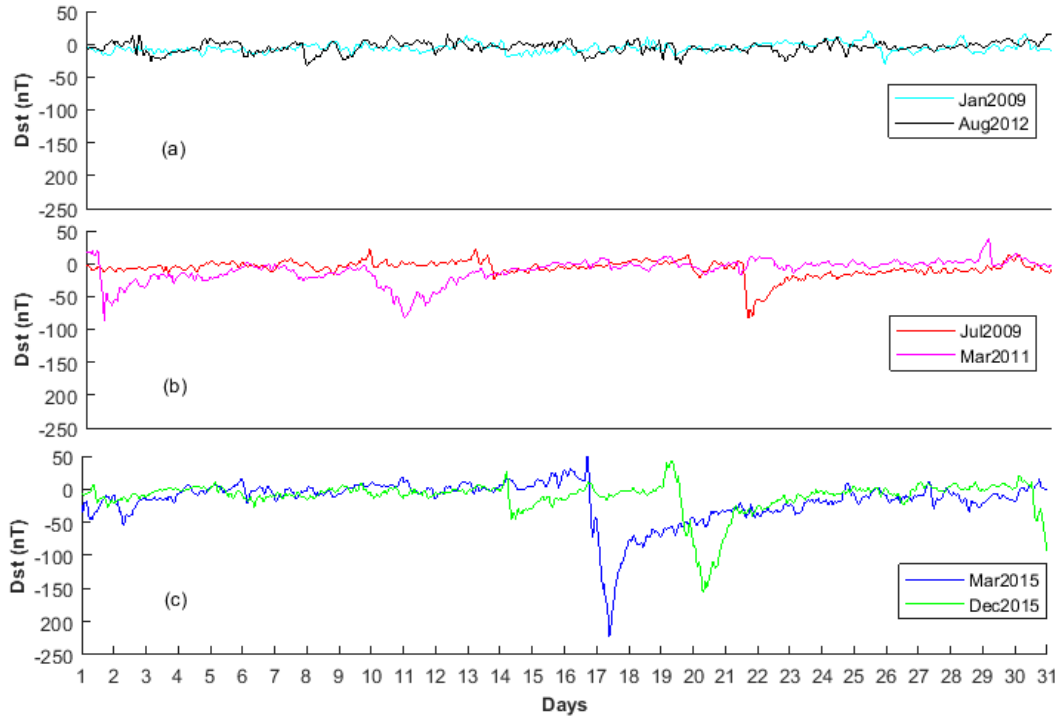
Figure 1: Samples of $D_{st}$ signals classified as (a) Minor, (b) Moderate and (c) Major geomagnetic
storm

678
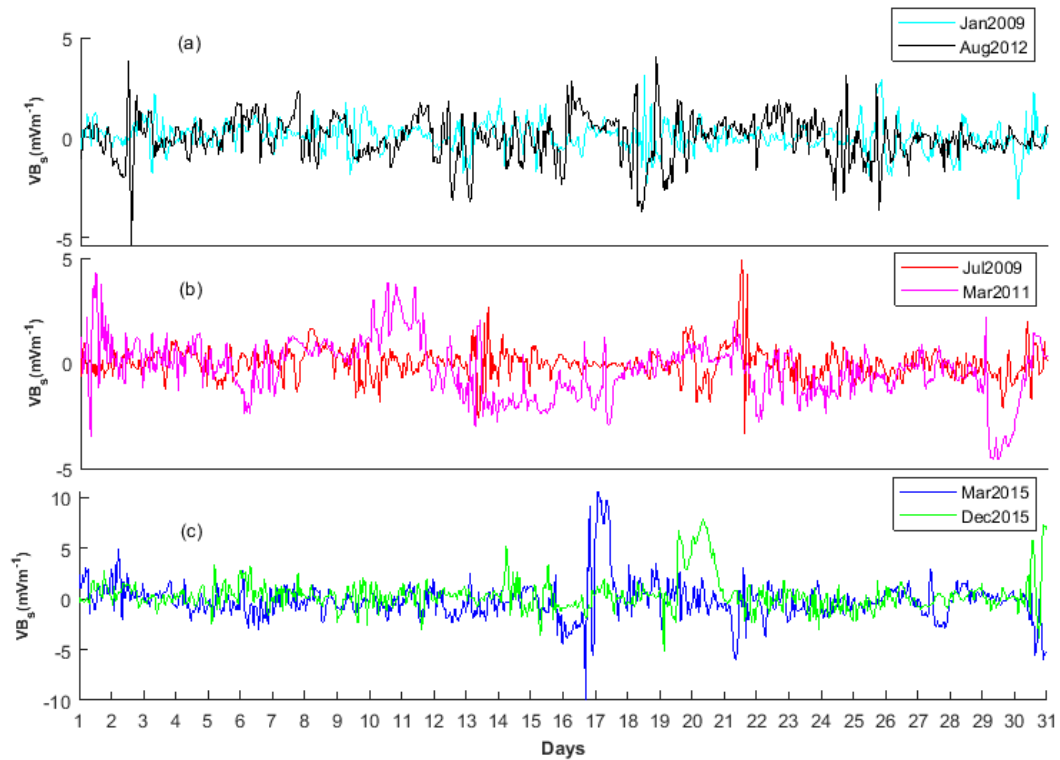
Figure 2: Samples of solar wind electric fields $(VB_s)$ during (a) Minor, (b) Moderate and (c) Major
geomagnetic storm.

681
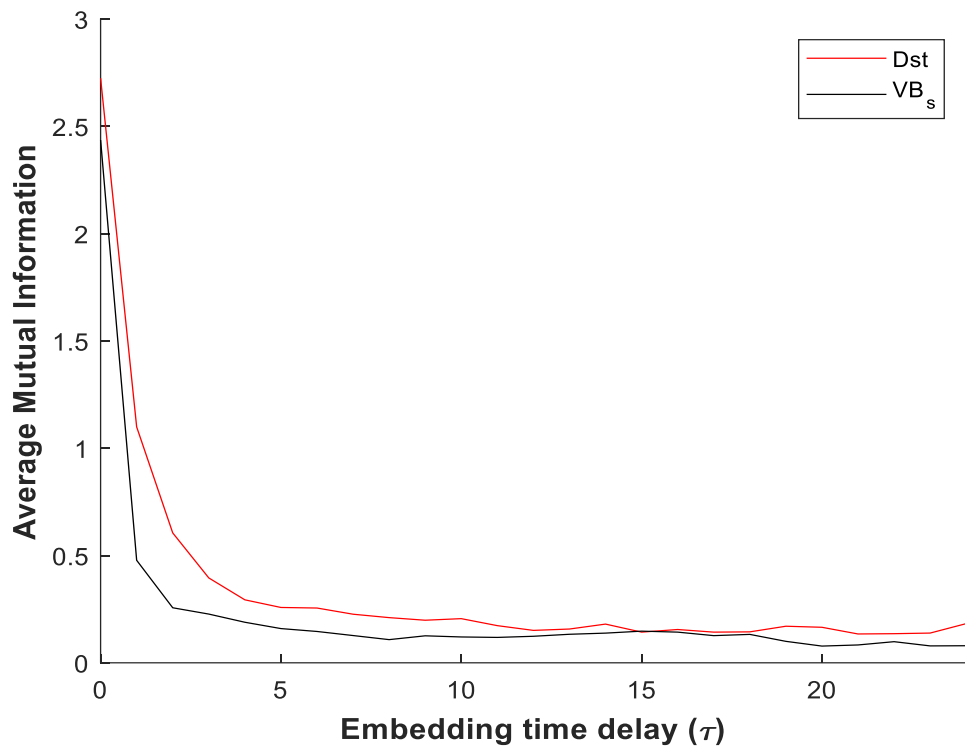
682

683    Figure 3: The plot Average Mutual Information against embedding time delay ($\tau$)
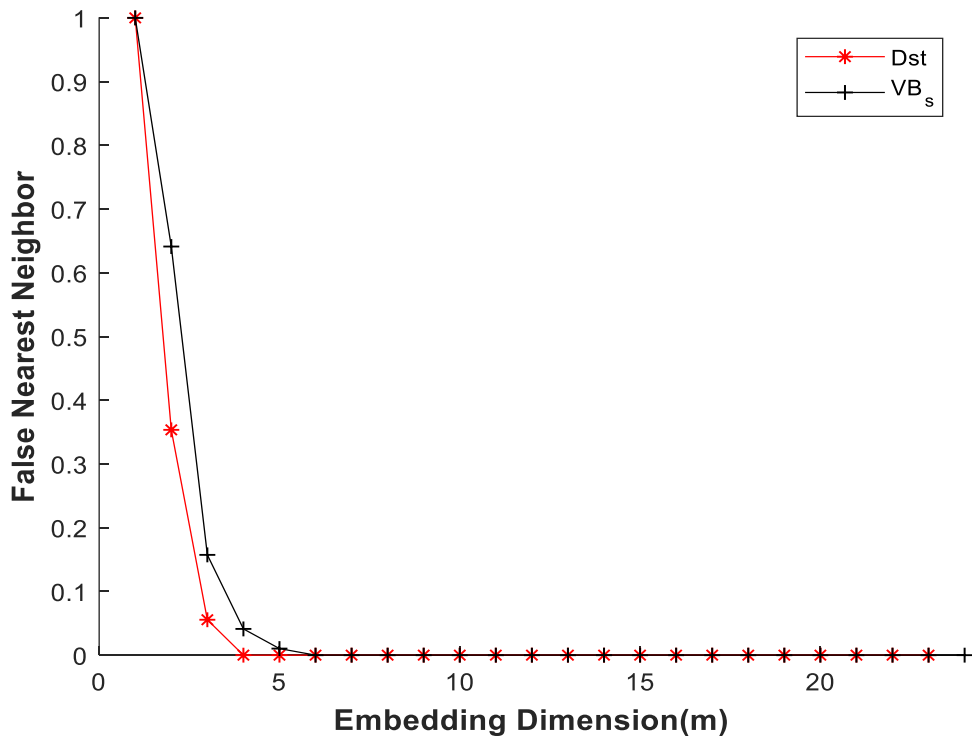
684

685    Figure 4: The plot of Percentage of False Nearest Neighbors against embedding dimension ($m$)
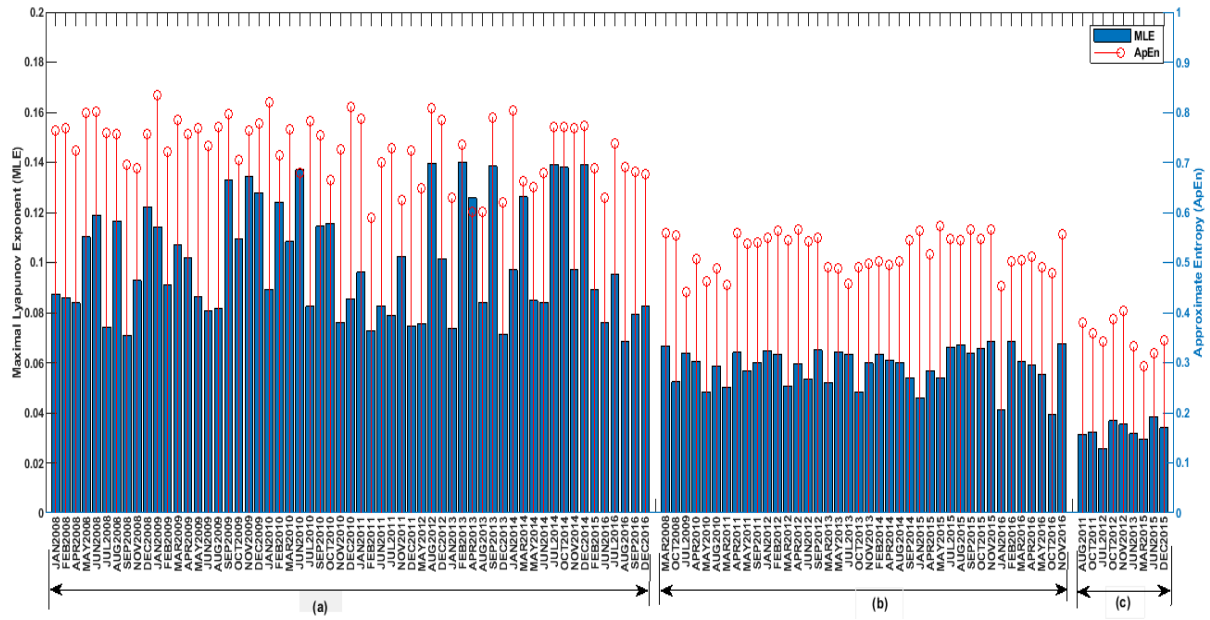
Figure 5: The MLE (bar plot) and ApEn (stem plot) of $D_{st}$ at: (a) Minor, (b) Moderate and (c) Major geomagnetic storm.
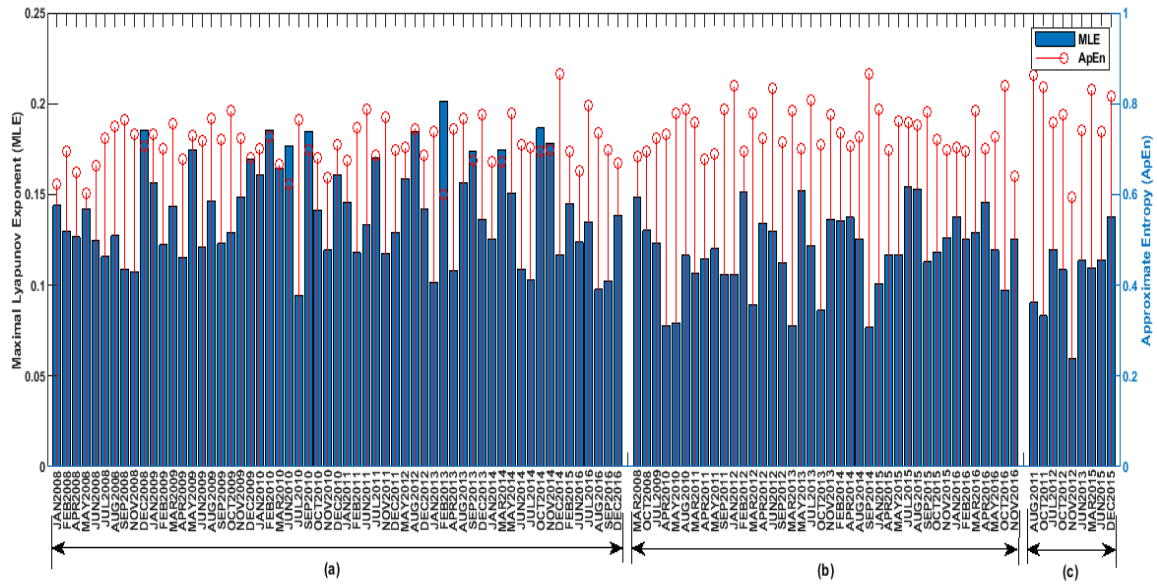
Figure 6: The MLE (bar plot) and ApEn (stem plot) of solar wind electric field ($VB_s$) during: (a) Minor, (b) Moderate and (c) Major geomagnetic storm.
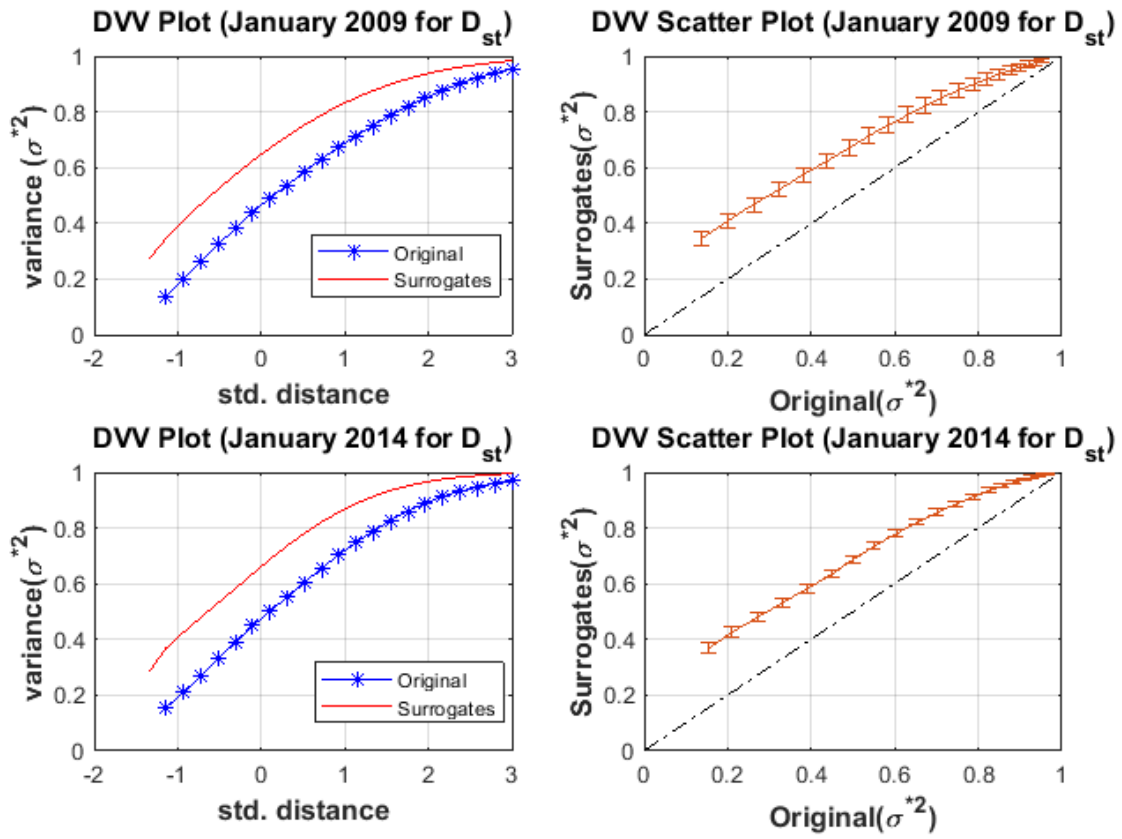
712

713     Figure 7: The DVV plot and Scatter plot for $D_{st}$ during  minor geomagnetic storm for January
714     2009 and January 2014.

715

716
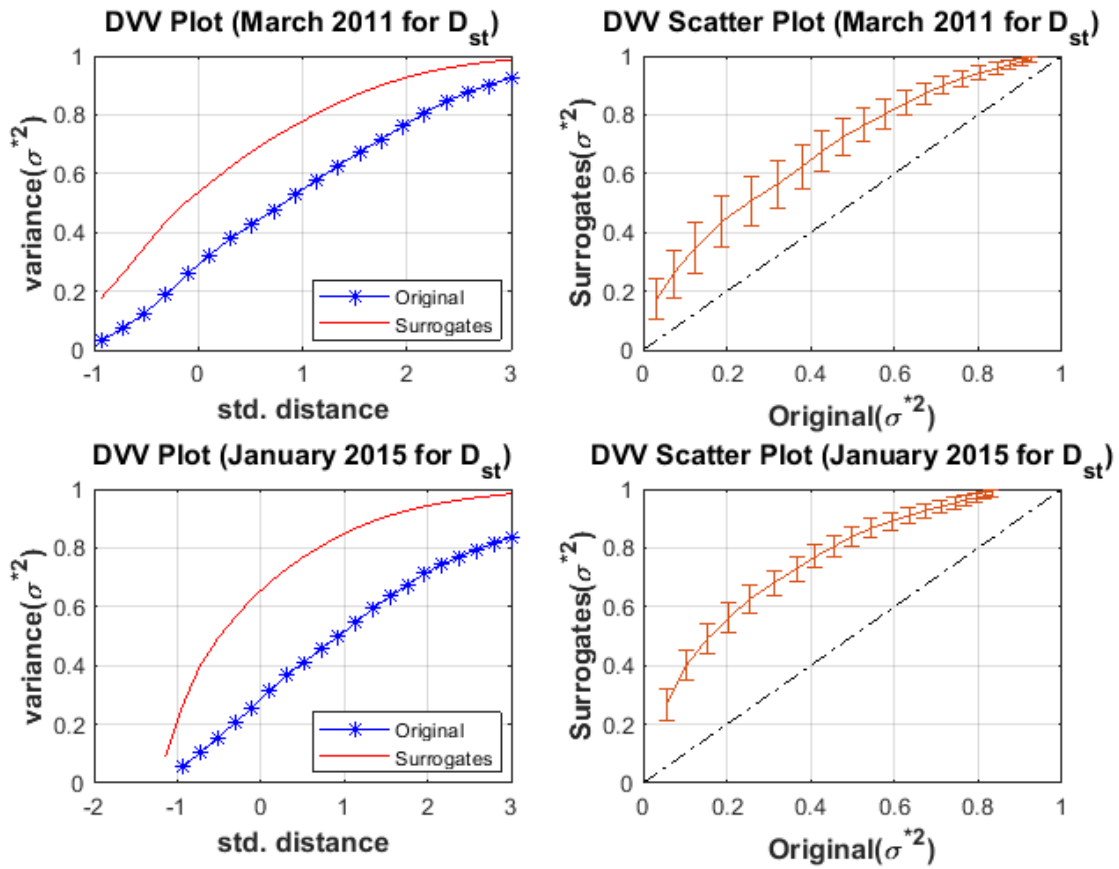
Figure 8: The DVV plot and Scatter plot for $D_{st}$ during moderate geomagnetic storm for March
2011 and January 2015.

719
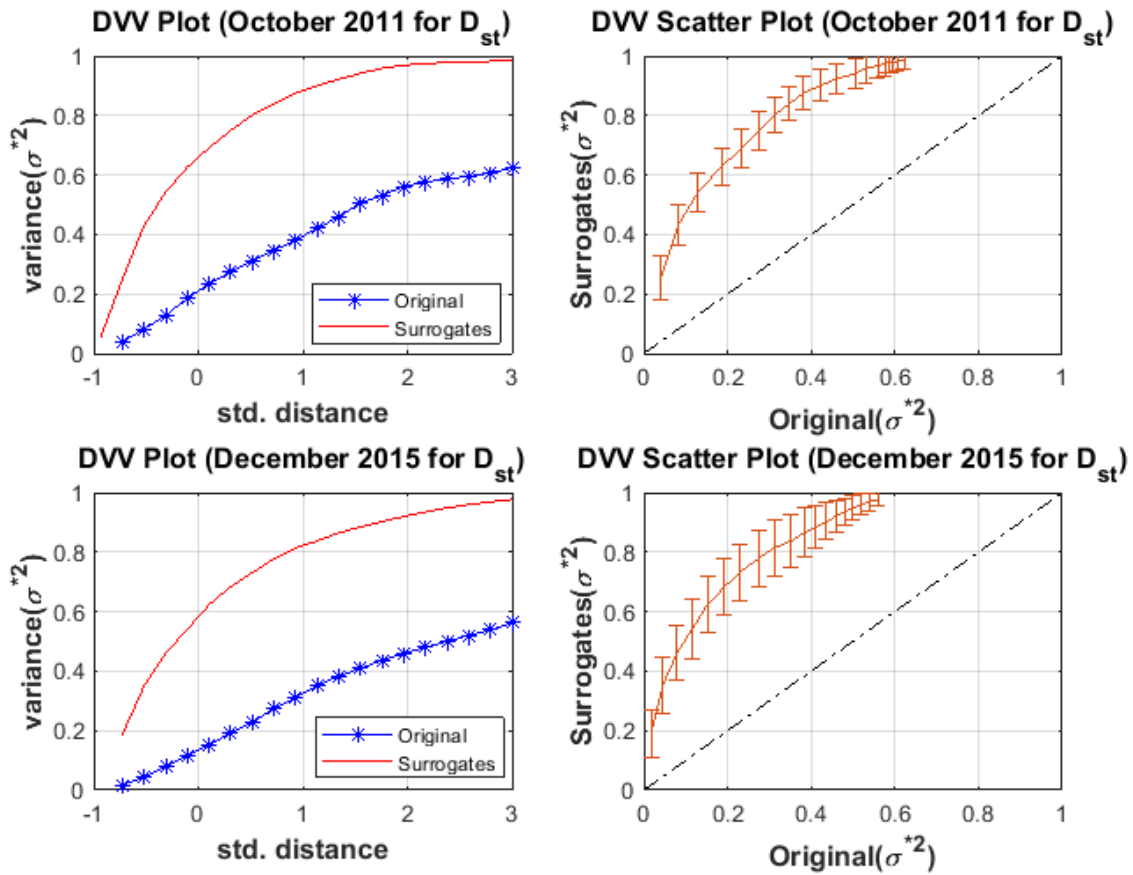
720

721  Figure 9: The DVV plot and Scatter plot for $D_{st}$ during major geomagnetic storm for October
722  2011 and December 2015.

723

724
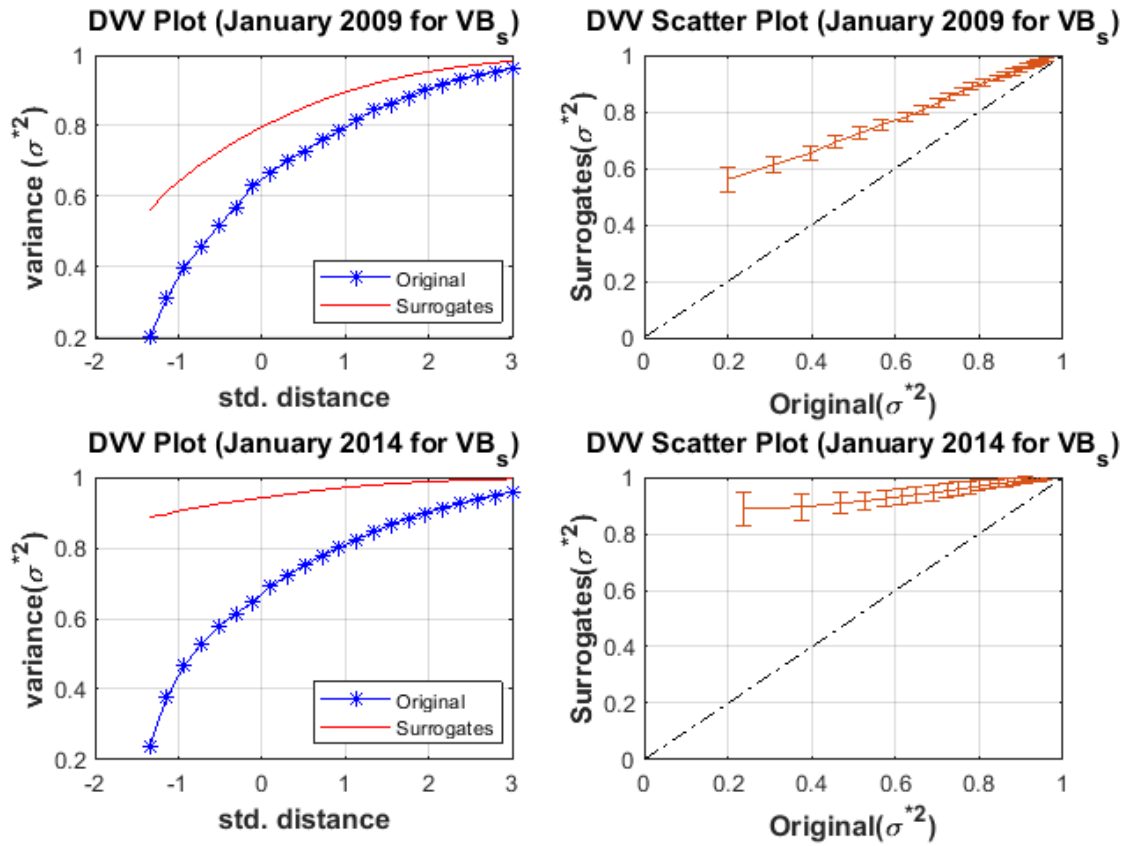
Figure 10: The DVV plot and Scatter plot for $VB_s$ during minor geomagnetic storm for January
2009 and January 2014.

727

728
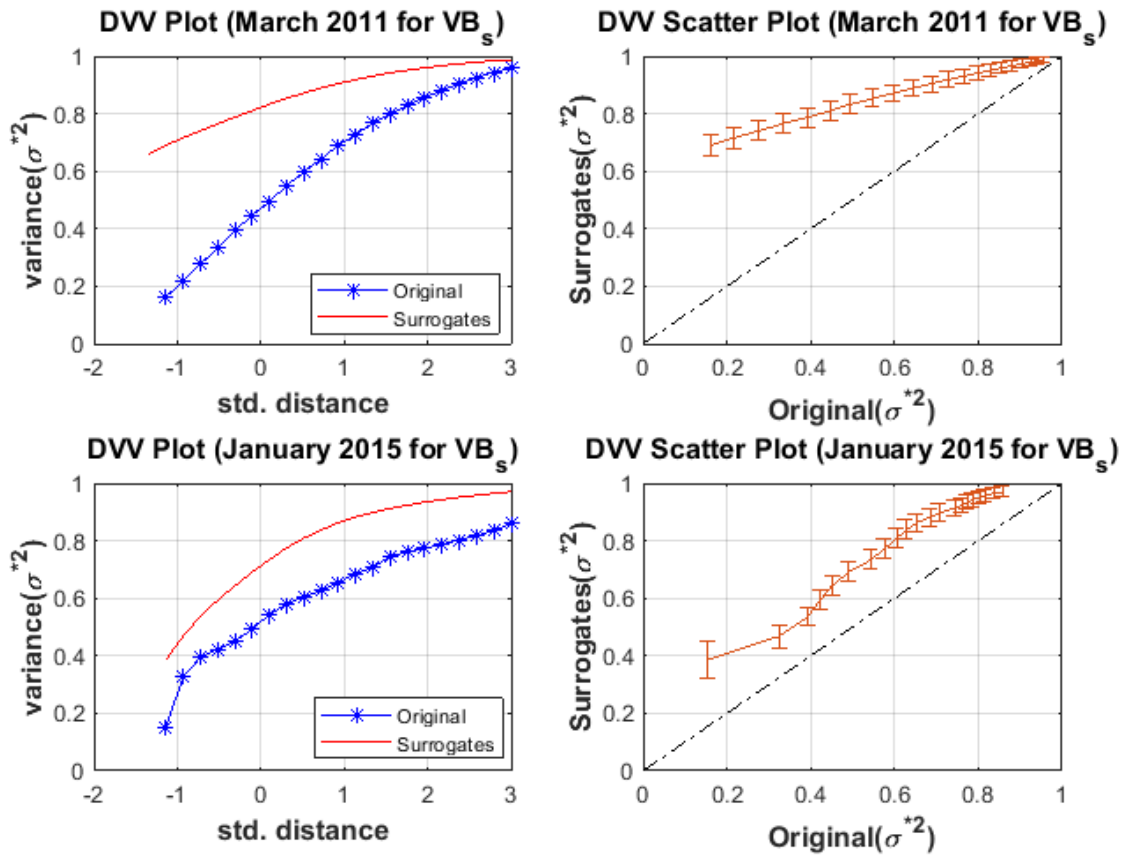
729

730  Figure 11: The DVV plot and Scatter plot for $VB_s$ during moderate geomagnetic storm for March
731  2011 and January 2015.

732

733
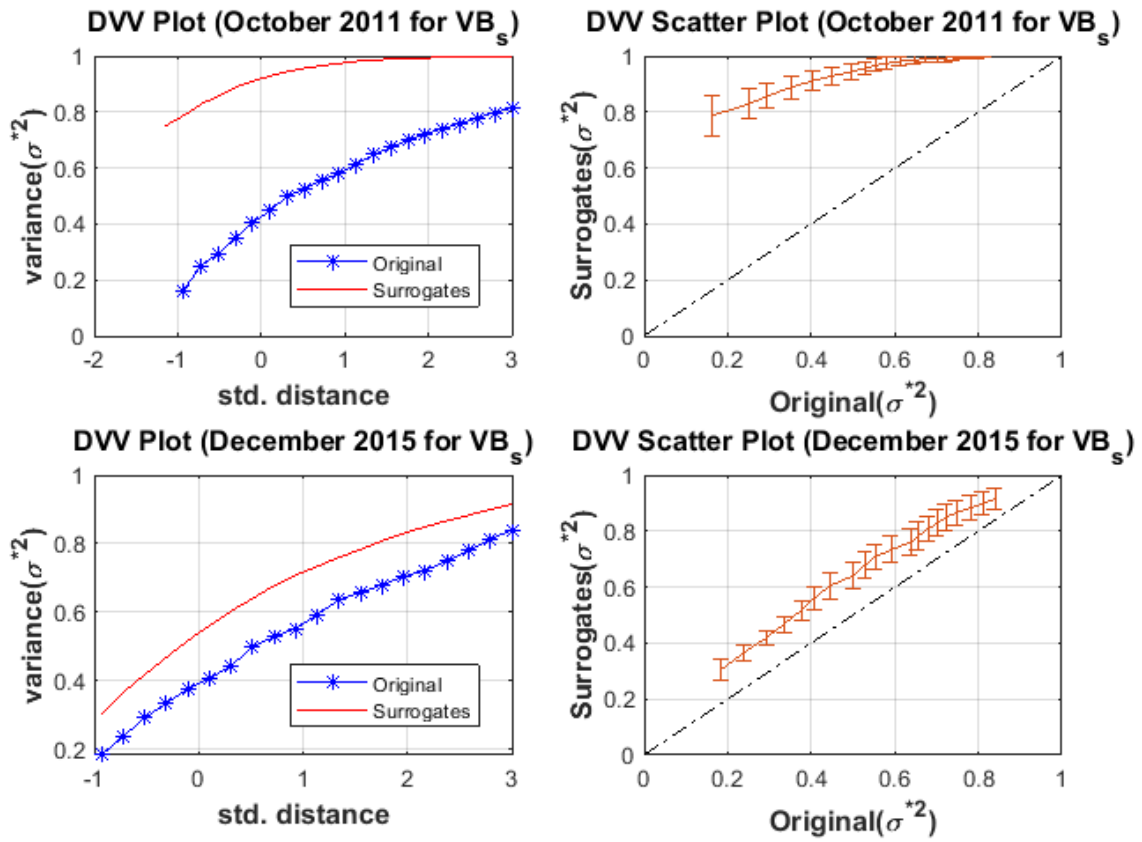
734

735 Figure 12: The DVV plot and Scatter plot for $VB_s$ during major geomagnetic storm for October
736 2011 and December 2015.

737

738

739